Progress In Electromagnetics Research B, Vol. 13, 59–74, 2009

TEM HORN ANTENNA FOR ULTRA-WIDE BAND MICROWAVE BREAST IMAGING

R. K. Amineh, A. Trehan, and N. K. Nikolova

Department of Electrical and Computer Engineering
McMaster University
1280 Main St. W., Hamilton, ON L8S 4K1, Canada

Abstract—A novel TEM horn antenna placed in a solid dielectric medium is proposed for microwave imaging of the breast. The major design requirement is that the antenna couples the microwave energy into the tissue without being immersed itself in a coupling medium. The antenna achieves this requirement by: 1) directing all radiated power through its front aperture, and 2) blocking external electromagnetic interference by a carefully designed enclosure consisting of copper sheets and power absorbing sheets. In the whole ultra-wide band the antenna features: 1) good impedance match, 2) uniform field distribution at the antenna aperture, and 3) good coupling efficiency.

1. INTRODUCTION

The non-ionizing microwave radiation is potentially useful means of detecting malignant tumors in the breast. The contrast between the dielectric properties of the healthy breast tissue and malignant tumors is the basis of this detection. Approaches to microwave breast imaging have recently attracted increased interest due to advances in both hardware and imaging algorithms (e.g., see [1–7]). Active microwave imaging techniques include tomographic techniques (e.g., see [1]) and radar-based techniques (e.g., see [7]).

The design and fabrication of high-performance antennas present significant challenges in the implementation of both categories of microwave imaging. An important antenna design requirement is a wide impedance bandwidth. In radar-based techniques, the wide bandwidth is a prerequisite to achieving high fidelity of the radiated

Corresponding author: R. K. Amineh (khalajr@mcmaster.ca).

pulse. In tomographic techniques, the frequency-hopping approach is used which employs multi-frequency microwave measurements. It allows for the reconstruction of the permittivity distribution with higher fidelity compared to a single-frequency or narrow-band reconstruction [8]. Other typical design requirements that have been considered in the literature are high directivity as well as small size so that a number of antennas could be positioned around the breast. Various types of antennas have been proposed for tissue-sensing applications. Typical examples include planar monopole [9], slot antenna [10], Fourtear antenna [11], microstrip patch antenna [12], planar "dark-eyes" [13], and ridged pyramidal horn [14].

For microwave scanning of the breast, the antennas and the tissue are typically immersed in a coupling liquid with dielectric properties as close as possible to the average properties of the breast tissue in the operating frequency band (e.g., see [15]). This medium minimizes the reflections occurring at the skin interface and increases the penetration into the tissue. Optimizing the coupling liquid based on *in vivo* measurement data has been addressed in [15] where the coupling liquid is a mixture of glycerin and water. Also, several liquids have been compared in [16] and the benefits of selecting an oil-based immersion liquid have been discussed. However, the selection of a convenient and practical coupling medium for realistic clinical experiments is still an issue of debate. The coupling medium complicates maintenance and requires replacement to avoid contamination.

Here, an ultra-wide band (UWB) TEM horn antenna placed in a partially shielded dielectric medium is proposed. The major design consideration, which distinguishes this antenna from the previously proposed antennas for this application are: (1) elimination of the coupling liquid, (2) directing all radiated power toward the tissue via the front aperture of the antenna, and (3) blocking the electromagnetic interference from the surrounding medium by a carefully designed enclosure consisting of copper sheets and power absorbing sheets. The first requirement ensures that the imaging system is convenient to use in a clinical environment, i.e., that it is easy to maintain and sanitize the apparatus after a patient is examined. The second and third requirements are crucial in the detection and characterization of tumors. The antenna also features ultra wide impedance bandwidth. It is designed to operate in the UWB range allowed by the Federal Communication Commission (FCC) for indoor applications, i.e., 3.1 GHz to 10.6 GHz. The amount of power coupled to the tissue through the front aperture is quantified by a new parameter called near-field directivity (NFD). To compute NFD, instead of computing near-field directivity for each point as proposed in [17], the integration

of the real part of the Poynting vector is computed over a surface overlapping the antenna aperture and the result is divided by the total radiated power. The overall ability to couple power into the tissue is quantified by a related parameter, the coupling efficiency.

Impedance match of the antenna in the UWB frequency range has been demonstrated by both simulation and experimental results. Excellent NFD factor has been obtained when simulating the performance of the antenna. Also, excellent decoupling from the surrounding medium for the antenna has been demonstrated by experimental investigations.

Furthermore, we propose a modification in the design to provide a uniform distribution of the radiated power over the antenna aperture. The proposed antenna enables the design of a new microwave imaging system where coupling liquid is not required.

2. DESCRIPTION OF THE ANTENNA STRUCTURE

The TEM horn antenna consists of two flared metallic plates. The flare angle, plate width and length are major design parameters that allow efficient radiation when chosen properly. For broadband performance, tapering of the distance between the two plates and the width of the plates [18, 19] is often used. Here, a linearly tapered structure is used, as shown in Figure 1, because of its fabrication simplicity. Here, we consider feeding the TEM horn antenna by the coaxial line. A balun is placed between the coaxial line and the two plates of the TEM horn in order to match the impedance of the horn to that of coaxial line. Our goal is to design the balun and the TEM horn antenna such that the whole radiating structure covers the entire UWB.

A microstrip-type balun is used as proposed in [18] and illustrated in Figure 1. The upper plate of the balun is connected to the coaxial core and its width is tapered away from the feed point. The lower plate is connected to the coaxial shield and its width is also tapered. Thus, the impedance of the balun gradually transits from that of the coaxial line to that of the parallel plates. The balun parameters influence significantly the impedance match of the antenna.

This TEM horn is placed in a solid dielectric medium, as shown in Figure 2, with $\varepsilon' = 10$ and $\tan\delta = 0.01$ (ECCOSTOCK HiK Cement, Emerson & Cuming Microwave Products) so that it can be used for direct measurement of the breast tissue without a coupling liquid. The latter is an important requirement of the imaging system. Permittivity of 10 has been chosen so that the antenna can be used for microwave imaging of the breast for various patients. The measured permittivity results reported in [20] reveals that for patients with dense

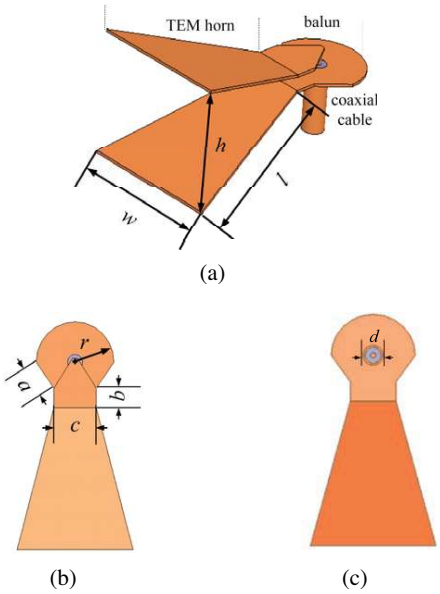

Figure 1. (a) The TEM horn with a coaxial feed and the balun. (b) Top view of the TEM horn. (c) Bottom view of the TEM horn.

breasts (comprising of mostly fibroglandular tissue) the permittivity is much higher and in the order of 20 or 30. This is the case where low-permittivity coupling medium fails to reduce reflections from the medium-tissue interface. Generally, the permittivity is a designable parameter and the reflections from the front aperture influence the UWB impedance bandwidth. In principle, higher permittivities for the dielectric medium lead to a smaller aperture and a shorter horn. This is because for certain electrical lengths, higher permittivities lead to lower wavelengths and ultimately smaller dimensions.

The shape parameters of the dielectric enclosure also influence the impedance of the antenna. In order to decouple the antenna from the surrounding medium, the outer surface of the dielectric enclosure is covered with copper sheets on the top, bottom, and side surfaces. These copper sheets are bonded together. The top and bottom copper sheets have patterned apertures [see Figure 2] in order to tune the impedance in the UWB range. The areas that are not covered by copper sheets are shown in pink (lighter gray in gray scale) in Figure 2. Note that the bottom copper sheet is very close to the coax shield but is not connected to it. In the tuning process, which was performed experimentally, it was observed that each aperture improves

the impedance match in a particular portion of the UWB. Apertures in the top copper shield are centered in the sheet with respect to the y direction. It is believed that (1) these apertures change the field distribution around the feed point such that the antenna reactance reduces and (2) slight radiation is occurred via these apertures which leads to better match for the antenna radiation resistance. However, this radiation is absorbed by a microwave absorbing sheet with $\varepsilon' \approx 30$, $\varepsilon'' \approx 2$, $\mu' \approx 1.7$, and $\mu'' \approx 2.7$ (ECCOSORB FGM-40, Emerson & Cuming Microwave Products) which is glued to the top surface. This prevents undesired radiation and interference.

3. SIMULATION AND MEASUREMENT RESULTS

The design of the TEM horn is carried out with HFSS ver. 11 [21]. In the simulation model, the surrounding medium is air except for the front side of the antenna which is in contact with a simplified breast model consisting of two infinite layers — skin layer and tissue layer

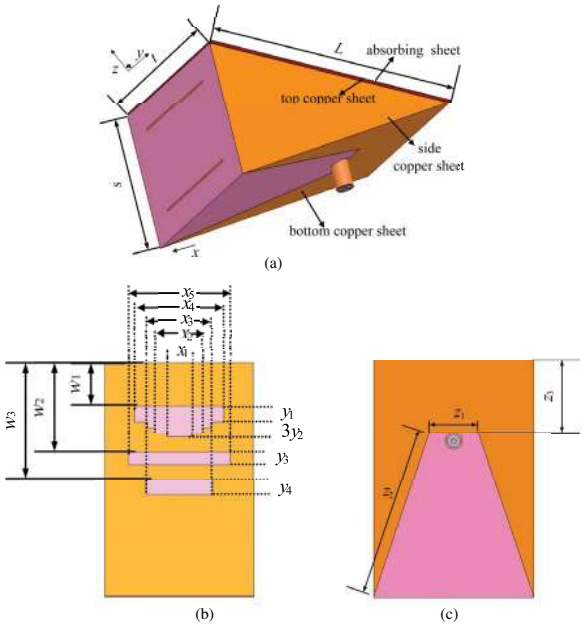

Figure 2. (a) The TEM horn enclosed in a dielectric medium with relative permittivity of 10 with copper sheets on all outer surfaces except the front aperture and a microwave absorbing sheet on the top surface. (b) The copper sheet pattern on the top surface. (c) The copper sheet pattern on the bottom surface.

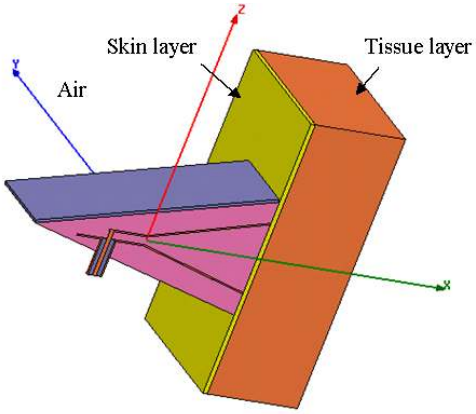

Figure 3. Cross section of simulation setup.

[see Figure 3]. In order to assign properties to these two layers in the simulation, first two artificial glycerin phantoms for tissue and skin layers are made with thicknesses of 5 cm and 1.5 mm, respectively. The reported dielectric properties of the breast tissues in [20] are considered when making the phantoms. The dielectric properties of these phantoms are measured with Agilent 85070E Performance Dielectric Probe Kit. Figure 4 shows the measured relative permittivity and effective conductivity of the phantoms. These properties are used in the HFSS simulations. Also, a lump port excitation has been used in HFSS simulations at the lower end of the coaxial cable.

In the first step, the balun and the TEM horn antenna were designed using the formulas presented in [18] applied in the case of a dielectric medium with permittivity of 10. In the second step, the design parameters were tuned using EM simulations in order to achieve good impedance match in the whole UWB. Since this antenna is in a finite dielectric medium and has a patterned shield, significant changes in the design parameters were required. An attempt has been made to keep the front of the antenna as small as possible without compromising the UWB performance so that arrangements of 4 to 6 array elements around the breast are possible. Table 1 shows the parameters of the designed antenna. The antenna length is 75 mm and the aperture size is 38 mm $\times$ 47 mm.

The S-parameter measurements are carried out with an Advantest R3770 Vector Network Analyzer (VNA). Since the antenna has a 3.5 mm (F) connector, the VNA is calibrated with its electronic calibration kit Advantest Auto CAL Kit 3.5MM F/F ADV R17051A. The performance of the antenna is investigated experimentally by

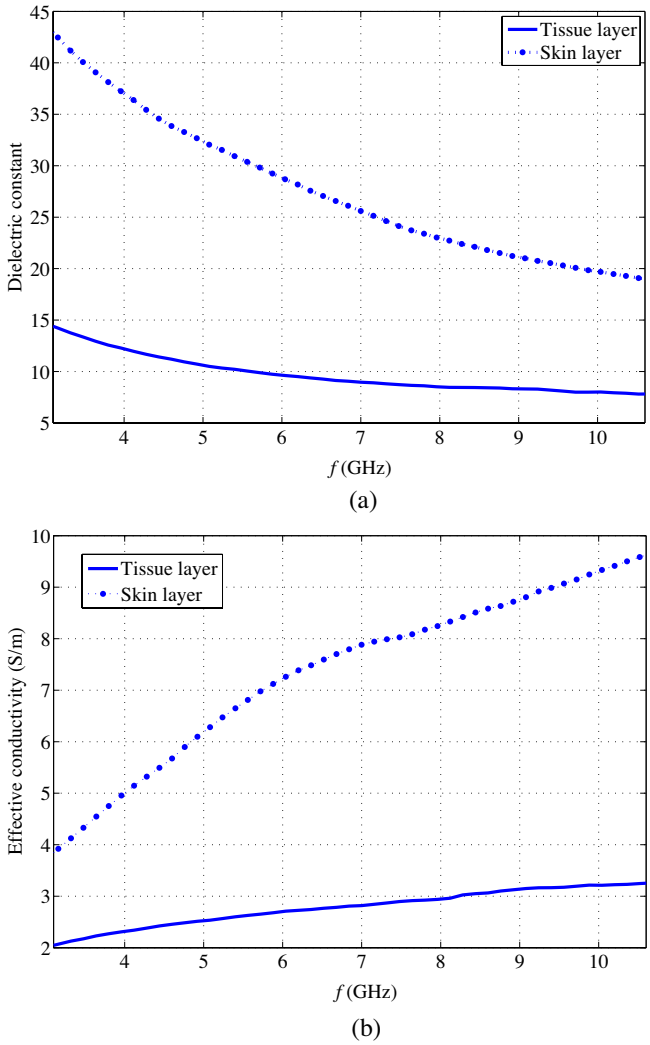

Figure 4. Constitutive parameters of the tissue and skin phantoms: (a) dielectric constant and (b) effective conductivity.

measuring: (1) the tissue layer alone, (2) tissue layer and skin layer together, and (3) real breast[†]. Figure 5 compares the simulated return loss of the designed antenna with the measured results which are in fairly good agreement. This figure also shows the good performance of

[†] The breast of a volunteer is measured as the person is sitting. Since there is no need for immersion in a coupling medium, the antenna is directly pressed against the breast.

Table 1. Design parameters for the antenna.

Parameter	Value (mm)	Parameter	Value (mm)
l	39.6	w_3	38.0
w	31.2	x_1	8.0
h	22.6	x_2	21 .0
a	8.3	x_3	28 .0
b	5 .0	x_4	32.0
c	11.4	x_5	15.0
r	10.5	y_1	5.0
d	5.0	y_2	2.0
L	75.9	y_3	4.0
s	38.0	y_4	5.0
t	47.0	z_1	14.0
w_1	14.0	z_2	55.3
w_2	29.0	z_3	23.0

the antenna in the whole UWB band when measuring both phantoms and human breast. The observed resonances in the $|S_{11}|$ response are largely due to reflections from the skin interface (or the end of the horn) as well as the intrinsic resonances of the shielding. In fact, these resonances are crucial in achieving the impedance match in the whole UWB. It is often the case with TEM horns that the reflection coefficient $|S_{11}|$ has many resonances in the UWB. Since the proposed antenna has more complicated structure than a TEM horn in open space, more resonances can be expected, which depend on the dimensions and the constitutive parameters of the dielectric medium, the shielding, and the balun.

In order to investigate the amount of power coupled to the tissue, we define a near-field directivity (NFD) factor for the antenna. For this purpose, we compute the power radiated from the surfaces of a cuboid surrounding the antenna with a size of $103\,\text{mm} \times 90\,\text{mm} \times 90\,\text{mm}$ as well as the radiated power through the face with the size of $90\,\text{mm} \times 90\,\text{mm}$ overlapping the front face of the antenna. Then NFD is computed as

$$\text{NFD} = P_f / P_T \tag{1}$$

where P_f is the power radiated through the front of the antenna and P_T is the total power radiated through the surface of the cuboid[‡]. Figure 6 shows the simulated NFD factor for the designed antenna. More than 90% of the total power is radiated via the front side toward the tissue. This simulation is performed with the setup shown in Figure 3.

[‡] The radiated power is computed as the flux integral of the real part of the Poynting vector $0.5(\mathbf{E} \times \mathbf{H}^*)$ over the respective surface.

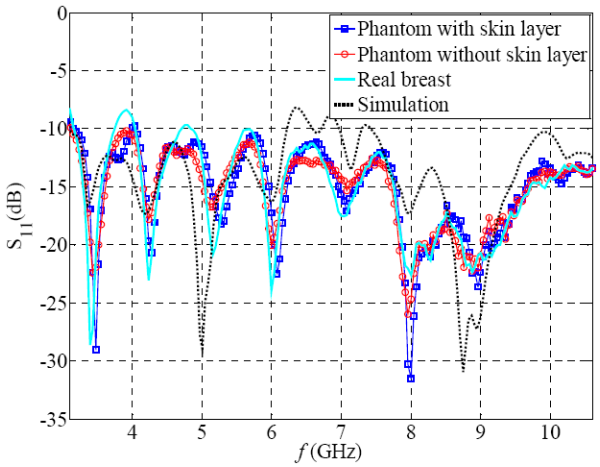

Figure 5. Comparison of the simulated and the measured return loss for the antenna.

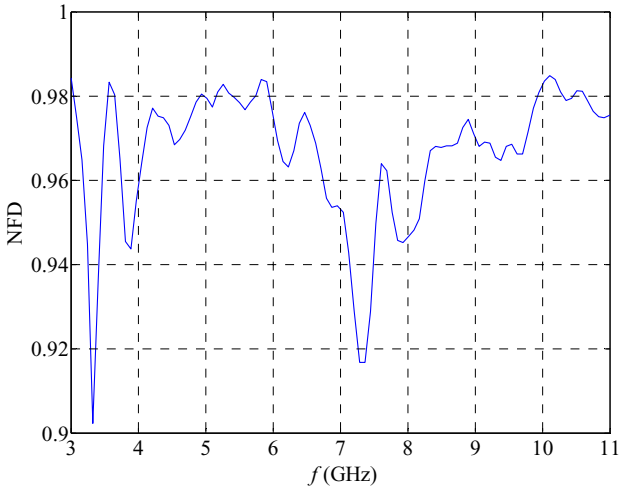

Figure 6. Simulated NFD for the antenna.

Also, the radiation efficiency is computed which is defined as $e_{\text{rad}} = P_T/P_{\text{in}}$ where P_T is the radiated power as defined above and P_{in} is the power fed to the antenna (i.e., the incident power minus the reflected power computed from the reflection coefficient S_{11}), as proposed in [13]. The average radiation efficiency over the UWB is 55%. Then, we define the coupling efficiency as $e_c = e_{\text{rad}} \times \text{NFD} =$

P_f/P_{in} which shows the fraction of the input power that is coupled to the tissue through the antenna aperture. The average radiation efficiency over the UWB is more than 50%. This indicates that the overall coupling efficiency of the proposed antenna is much better than

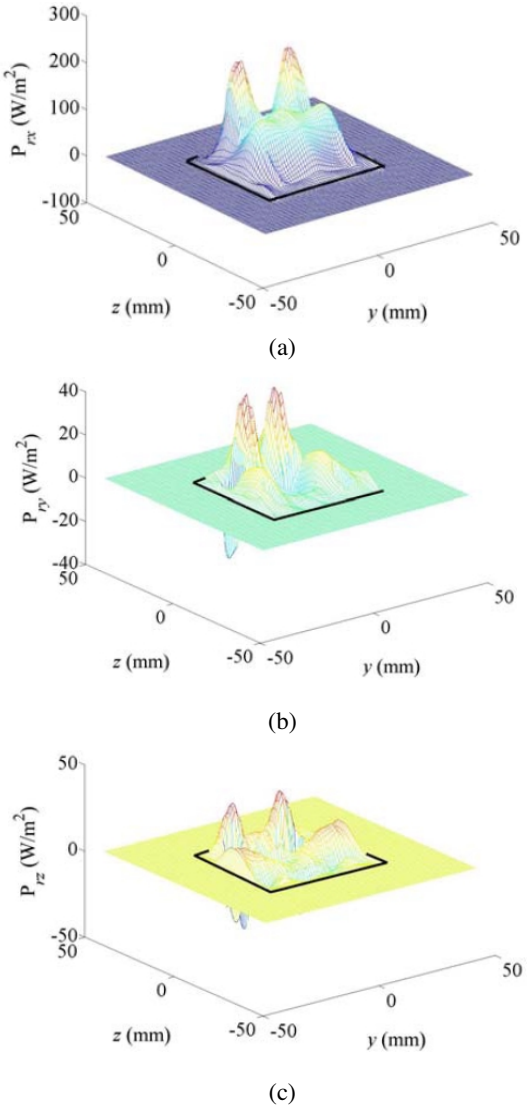

Figure 7. The components of the real part of the Poynting vector at 6 GHz: (a) x-component, (b) y-component, (c) z-component. The solid line shows the projection of the antenna aperture on this plane.

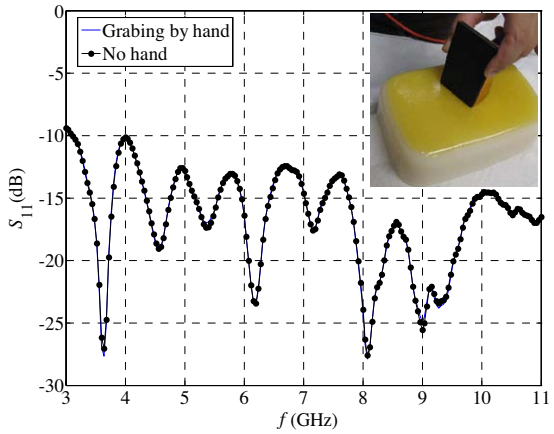

Figure 8. Measuring the breast phantom when grabbing the antenna directly.

that of existing low-directivity UWB antennas whose average radiation efficiencies e_{rad} are of comparable values; for example, see [13]. Note that a non-directional UWB antenna requires coupling liquid in order to achieve good energy coupling to the tissue and to minimize EM interference. The proposed antenna achieves both without the need for coupling liquid.

In order to investigate the power density distribution at the antenna aperture, we have plotted in Figure 7 the components of the real part of the Poynting vector at 6 GHz. Integration of the x-, y-, and z-components of the real part of the Poynting vector over the antenna aperture gives the values of $0.49\,\text{W/m}^2$, $-0.002\,\text{W/m}^2$, and $0.03\,\text{W/m}^2$, respectively. This shows that the x-component (which is normal to the front aperture) contains the major amount of radiated power compared with the other components. The same is true throughout the UWB.

It is worth noting that the size of the cuboid surrounding the antenna in the simulations does not affect the computed total radiated power. The size of the front side of the cuboid overlapping the antenna aperture does not influence significantly the computed power leaving the front surface either. The reason is that the radiated power over the front side of cuboid is mostly confined to the antenna aperture as shown in Figure 7.

The proposed antenna is very well isolated from the outside environment. In fact, its performance does not change even when the measurement is performed by grabbing the antenna directly by hand as shown in Figure 8.

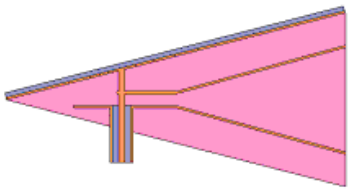

Figure 9. Cross section view showing the connection of the top plate of the horn to the top copper shielding sheet.

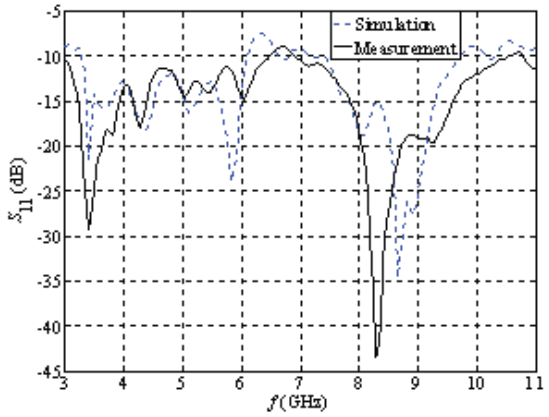

Figure 10. Simulated and measured return loss for the modified antenna.

4. IMPROVING THE APERTURE FIELD DISTRIBUTION

In Figure 7(a), we observe that the power density distribution is irregular. In particular its intensity is high in the region between the top TEM horn plate and the top copper shield. To prevent that, we introduce a connecting wire between these two plates as shown in Figure 9. Thus, propagating modes between the two top plates are suppressed. Simulated and experimental results confirm that the modified antenna still has a good return loss [Figure 10] and excellent NFD in the whole UWB. However, the power density distribution at the antenna aperture is now more uniform. Figure 11 shows the x-component of the real part of the Poynting vector at 6 GHz for the modified design. Comparing this figure with Figure 7(a) confirms that the power density distribution is more uniform in the modified design.

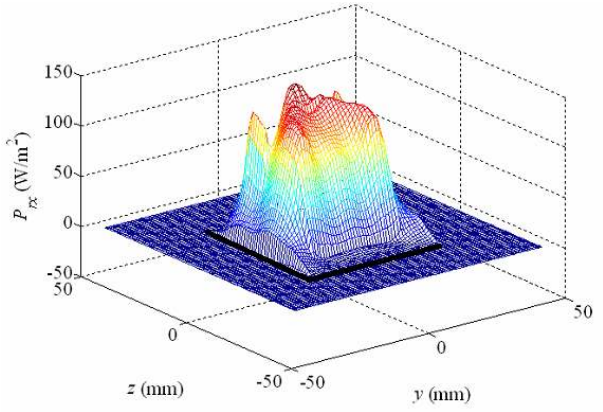

Figure 11. x-component of the real part of the Poynting vector at 6 GHz for the modified design. The solid line shows the projection of the antenna aperture on this plane.

5. CONCLUSION AND DISCUSSION

In this paper, a novel UWB TEM horn antenna placed in a dielectric medium has been proposed for microwave imaging in breast cancer detection. The outer surface of the antenna is covered by copper sheets and a microwave absorbing sheet. The design is accomplished through full-wave simulation and then experimentally tunned for best impedance match. Simulated and experimental results confirm that the following design requirements are met: (1) The antenna does not need to be immersed in a coupling liquid. (2) The near-field power is directed entirely toward the tissue through the front aperture of the antenna. (3) Excellent isolation from external electromagnetic interference (EMI) is achieved. (4) Good impedance match in the UWB frequency range is achieved. (5) The power density distribution over the antenna aperture is fairly uniform.

This antenna enables the development of practical imaging systems which will be easy to maintain in a clinical environment. Such systems will allow for convenient and fast sanitation of the equipment after a patient is examined.

Furthermore, the specifications stated in (2) and (3) are crucial for the sensitivity and the EMI immunity of the microwave breast imaging system that have not been properly addressed in previously reported work. We intend to use this antenna in a microwave breast tomography system although it may be also a good candidate for radar-based imaging systems.

ACKNOWLEDGMENT

The authors are indebted to Robert K. Zimmerman, Jr., a research engineer, for his help in fabricating the antenna prototype.

REFERENCES

1. Rubæk, T., P. M. Meaney, P. Meincke, and K. D. Paulsen, "Nonlinear microwave imaging for breast-cancer screening using Gauss-Newton's method and the CGLS inversion algorithm," *IEEE Trans. Antennas and Propag.*, Vol. 55, No. 8, 2320–2331, August 2007.
2. Woten, D. A., J. Lusth, and M. El-Shenawee, "Interpreting artificial neural networks for microwave detection of breast cancer," *IEEE Microwave Wirel. Components Lett.*, Vol. 17, No. 12, 825–827, December 2007.
3. Davis, S. K., B. D. Van Veen, S. C. Hagness, and F. Kelcz, "Breast tumor characterization based on ultrawideband microwave backscatter," *IEEE Trans. Biomed. Eng.*, Vol. 55, No. 1, 237–246, January 2008.
4. Zhang, H., S. Y. Tan, and H. S. Tan, "A novel method for microwave breast cancer detection," *Progress In Electromagnetics Research*, PIER 83, 413–434, 2008.
5. Fhager, A. and M. Persson, "Using *a priori* data to improve the reconstruction of small objects in microwave tomography," *IEEE Trans. Microwav. Theory Tech.*, Vol. 55, No. 11, 2454–2462, November 2007.
6. Yu, C., M. Yuan, J. Stang, E. Bresslour, R. T. George, G. A. Ybarra, W. T. Joines, and Q. H. Liu, "Active microwave imaging II: 3-D system prototype and image reconstruction from experimental data," *IEEE Trans. Microwav. Theory Tech.*, Vol. 56, No. 4, 991–1000, April 2008.
7. Klemm, M., I. J. Craddock, J. A. Leendertz, A. Preece, and R. Benjamin, "Improved delay-and-sum beamforming algorithm for breast cancer detection," *Int. J. Antennas and Propag.*, Vol. 2008, Article ID 761402.
8. Chew, W. C. and J. H. Lin, "A frequency-hopping approach for microwave imaging of large inhomogeneous bodies," *IEEE Microw. Guided Wav. Lett.*, Vol. 5, No. 12, 439–441, December 1995.
9. Jafari, H. M., M. J. Deen, S. Hranilovic, and N. K. Nikolova, "A study of ultrawideband antennas for near-field imaging," *IEEE*

Trans. Antennas and Propag., Vol. 55, No. 4, 1184–1188, April 2007.

10. Jafari, H. M., J. M. Deen, S. Hranilovic, and N. K. Nikolova, "Co-polarised and cross-polarised antenna arrays for breast, cancer detection," *IET Microw. Antennas Propag.*, Vol. 1, No. 5, 1055–1058, October 2007.
11. Woten, D. A. and M. El-Shenawee, "Broadband dual linear polarized antenna for statistical detection of breast cancer," *IEEE Trans. Antennas and Propag.*, Vol. 56, No. 11, 3576–3580, November 2008.
12. Nilavalan, R., I. J. Craddock, A. Preece, J. Leendertz, and R. Benjamin, "Wideband microstrip patch antenna design for breast cancer tumour detection," *IET Microw. Antennas Propag.*, Vol. 1, No. 2, 277–281, April 2007.
13. Kanj, H. and M. Popovic, "A Novel ultra-compact broadband antenna for microwave breast tumor detection," *Progress In Electromagnetics Research*, PIER 86, 169–198, 2008.
14. Li, X., S. C. Hagness, M. K. Choi, and D. Van Der Weide, "Numerical and experimental investigation of an ultra-wideband ridged pyramidal-horn antenna with curved launching plane for pulse radiation," *IEEE Antennas Wirel. Propag. Lett.*, Vol. 2, 259–262, 2003.
15. Meaney, P. M., M. W. Fanning, T. Raynolds, C. J. Fox, Q. Fang, C. A. Kogel, S. P. Poplack, and K. D. Paulsen, "Initial clinical experience with microwave breast imaging in women with normal mammography," *Acad Radiol.*, Vol. 14, No. 2, 207–218, February 2007.
16. Sill, J. M. and E. C. Fear, "Tissue sensing adaptive radar for breast cancer detection: Study of immersion liquids," *Electron. Lett.*, Vol. 41, No. 3, 113–115, 2005.
17. Odendaal, J., J. Joubert, and M. J. Prinsloo, "Extended edge wave diffraction model for near-filed directivity calculations of horn antennas," *IEEE Trans. Instrument. and Measur.*, Vol. 54, No. 6, 2469–2473, December 2005.
18. Chung, K., S. Pyun, and J. Choi, "Design of an ultrawide-band TEM horn antenna with a microstrip-type balun," *IEEE Trans. Antennas and Propag.*, Vol. 53, No. 10, 3410–3413, October 2005.
19. Malherbe, J. A. G. and N. Barnes, "TEM horn antenna with an elliptic profile," *Microw. Opt. Tech. Lett.*, Vol. 49, No. 7, 1548–1551, July 2007.
20. Lazebnik, M., L. McCartney, D. Popovic, C. B. Watkins,

M. J. Lindstrom, J. Harter, S. Sewall, A. Magliocco, J. H. Booske, M. Okoniewski, and S. C. Hagness, "A large-scale study of the ultrawide band microwave dielectric properties of normal breast tissue obtained from reduction surgeries," *Phys. Med. Biol.*, Vol. 52, 2637–2656, May 2007.

21. Ansoft Corporation, USA, http://www.ansoft.com.